



HAL
open science

Effect of non-thermal plasma in the activation and regeneration of 13X zeolite for enhanced VOC elimination by cycled storage and discharge process

S. K. P. Veerapandian, N. de Geyter, Jean-Marc Giraudon, Jean-Charles Morin, P. S. E. Tabaei, G. de Weireld, A. Laemont, K. Leus, P. van der Voort, Jean-Francois Lamonier, et al.

► To cite this version:

S. K. P. Veerapandian, N. de Geyter, Jean-Marc Giraudon, Jean-Charles Morin, P. S. E. Tabaei, et al.. Effect of non-thermal plasma in the activation and regeneration of 13X zeolite for enhanced VOC elimination by cycled storage and discharge process. *Journal of Cleaner Production*, 2022, 364 (132687), 10.1016/j.jclepro.2022.132687 . hal-04053366

HAL Id: hal-04053366

<https://hal.univ-lille.fr/hal-04053366v1>

Submitted on 31 Mar 2023

HAL is a multi-disciplinary open access archive for the deposit and dissemination of scientific research documents, whether they are published or not. The documents may come from teaching and research institutions in France or abroad, or from public or private research centers.

L'archive ouverte pluridisciplinaire **HAL**, est destinée au dépôt et à la diffusion de documents scientifiques de niveau recherche, publiés ou non, émanant des établissements d'enseignement et de recherche français ou étrangers, des laboratoires publics ou privés.

1 **Effect of non-thermal plasma in the activation and regeneration of 13X zeolite for enhanced**
2 **VOC elimination by cycled storage and discharge process**

3
4 Savita Kaliya Perumal Veerapandian¹, Nathalie De Geyter¹, Jean-Marc Giraudon², Jean-Charles
5 Morin², Parinaz Saadat Esbah Tabaei¹, Guy De Weireld³, Andreas Laemont⁴, Karen Leus⁴, Pascal Van
6 Der Voort⁴, Jean-François Lamonier² and Rino Morent¹

7 ¹ *Ghent University, Faculty of Engineering and Architecture, Department of Applied Physics,*
8 *Research Unit Plasma Technology, Sint-Pietersnieuwstraat 41 B4, 9000 Ghent, Belgium*

9 *(*email: savita.kaliyaperumalveerapandian@ugent.be)*

10 ² *Univ. Lille, CNRS, Centrale Lille, Univ. Artois, UMR 8181 – UCCS – Unité de Catalyse et Chimie*
11 *du Solide, F-59000 Lille, France*

12 ³ *Université de Mons, Faculté Polytechnique, Service de Thermodynamique et de Physique*
13 *Mathématique, Place du Parc, 20, 7000 Mons, Belgium*

14 ⁴ *Ghent University, Department of Chemistry, COMOC-Center for Ordered Materials,*
15 *Organometallics and Catalysis, Krijgslaan 281-S3, 9000 Ghent, Belgium*

16
17
18
19
20
21
22
23
24
25
26
27
28

29 **Abstract.**

30 A non-thermal plasma (NTP) discharge is used in this study for the activation and regeneration of MS-
31 13X pellets packed in a MS-13X & glass beads packed bed dielectric barrier discharge (DBD) reactor.
32 NTP activation (*in-situ*) of MS-13X efficiently removes the adsorbed carbonaceous compounds and
33 moisture resulting in an improved VOC adsorption. In addition, NTP exposure is used for the
34 regeneration of the used MS-13X for cycled storage and discharge (CSD) removal of VOC from air.
35 The amount of adsorbed toluene, products formed and the surface and bulk properties of the regenerated
36 used MS-13X shows complete regeneration of used MS-13X. Finally, the stability of MS-13X during
37 10 cycles of CSD shows no degradation in performance. Thus, NTP exposure is proven to be successful
38 for both the activation and regeneration of MS-13X pellets used for cyclic CSD process.

39 **Keywords:** MS-13X, NTP activation, NTP regeneration, VOC abatement, Cycled storage and discharge

40 **Number of words:** 6591

41
42
43
44
45
46
47
48
49
50
51
52
53
54
55
56

571. Introduction

58 Most volatile organic compounds (VOCs) are toxic to human and environmental health [1]. Due
59 to their negative impact, it is important to reduce the emission of VOCs. Among the various
60 environmental processes which are used for the removal of VOCs from exhaust gases [2,3], adsorption
61 is one of the most cost effective and simplest process. The most commonly used adsorbents for VOC
62 removal are carbon based [4], and metal oxide-based adsorbents. However, the main limitations of
63 adsorption are the need for continuous regeneration of the used adsorbent, the disposal of spent
64 adsorbents and the processing of the adsorbed VOCs. In practice, most saturated sorbents are either
65 incinerated or disposed which leads to a negative impact on the environment. To make the adsorption
66 process more environmentally friendly and to reduce the demand for virgin adsorbents, it is thus
67 indispensable to regenerate the used adsorbents. Several processes which have been investigated for the
68 regeneration of adsorbents include pressure swing [5], temperature swing [6], microwave heating [6,7],
69 purging gas [6], chemical methods [5], and the combination of heating and catalytic oxidation [8]. In
70 addition, non-thermal plasmas (NTPs) have also been proven effective for the regeneration of spent
71 adsorbents [9,10], as NTPs generate ozone and N_2O which are very effective oxidizing agents.

72 Important adsorbent properties which have to be considered for pollution control include pore
73 size distribution, surface area, thermal stability and hydrophobicity. Due to their large specific surface
74 area, narrow pore size distribution and acidity, zeolites are very interesting candidates as adsorbents
75 [11]. In this particular work, zeolite X is used as adsorbent which is commercially available as MS-13X
76 (molecular sieve) in sodium (mostly) and calcium form. Zeolite 13X is a faujasite (FAU) molecular
77 sieve with a 3D pore structure, a pore size of $\sim 7 \text{ \AA}$ and an Si/Al ratio of $\sim 2.6-3$. The pore size of MS-
78 13X is suitable for the adsorption of various VOCs such as hexane, toluene, benzene, ethyl benzene, o-
79 , m-, p- xylene and methyl ethyl ketone (kinetic diameter in the range of $4.3 - 6.8 \text{ \AA}$) [12–14] and also
80 accessible for ozone (kinetic diameter of 5.8 \AA) [15] which is one of the oxidizing species produced by
81 an NTP.

82 This paper deals with the engineering of an original environmental process which combine (i)
83 adsorption and (ii) plasma discharge, which is known as a cycled storage and discharge (CSD) process

84 for the removal of VOCs from air. This environmental process involves two steps: first, the diluted VOC
85 is concentrated on the adsorbent (plasma off). Then, the adsorbed VOC is oxidized by NTP discharge.
86 The advantages of this process are: (i) reduced energy consumption by increasing the ratio of the
87 adsorption time to the plasma discharge time (particularly suitable for low concentration of VOC in a
88 large volume of exhaust gas), (ii) simultaneous oxidation of the adsorbed VOC and regeneration of the
89 adsorbent, avoids an extra step of regeneration and (iii) the possibility to use a benign discharge gas
90 which avoids the formation of unwanted and toxic by-products such as NO_x (which is out of scope for
91 this work).

92 In the past, Chao et al. investigated the decomposition of toluene using ozone in the presence of
93 13X zeolite [16] and reported the enhanced degradation of toluene, as the Lewis acid sites of the zeolite
94 decomposed ozone to form active oxygen which has a higher reactive rate constant when compared to
95 ozone [17]. However, the deactivation of the 13X zeolite occurred after a few hours of experiments. Yi
96 et al. investigated a metal loaded 13X zeolite for the removal of toluene using adsorption plasma
97 catalysis (APC) and reported that the catalytic activity and product selectivity were improved by the
98 metal loading [18]. In addition, Yi et al. also investigated the effect of a closed and ventilated discharge
99 on the oxidation of toluene adsorbed on a Co/13X zeolite and reported that the closed discharge was
100 more efficient for the oxidation of toluene [19]. Researchers investigated the use of bare 13X and metal
101 loaded 13X for the removal of various VOCs such as ethylene [20,21], benzene [22,23] and toluene
102 [23]. Researchers also investigated the use of different catalysts such as Mn-Cu/ Al_2O_3 [24] and CeO_2 -
103 $\text{Co}_3\text{O}_4/\gamma\text{-Al}_2\text{O}_3$ [25] for APC abatement of VOCs.

104 Although the above-mentioned research works established the use of MS-13X or metal loaded
105 MS-13X for APC or CSD removal of VOCs, these works have never investigated the effect of the used
106 NTP discharge on the surface and bulk properties of adsorbents in detail, which is critical for CSD
107 process. Apart from the stability of adsorbent in NTP discharge, the regenerability of adsorbent by NTP
108 has to be investigated as well. Thus, the main objective of this work is to investigate the use of an NTP
109 sustained in dry air for the activation of fresh MS-13X and the regeneration of used MS-13X for CSD
110 removal of toluene, a model VOC.

111 In the first part of this work, the adsorption capacity of MS-13X pellets activated by heating and
112 NTP discharge is compared. In the second part of this work, the use of NTP for the simultaneous
113 oxidation of adsorbed toluene and the regeneration of MS-13X pellets is studied. Then, the surface and
114 bulk properties of thermal activated, NTP activated and NTP regenerated MS-13X are studied. Based
115 on the obtained results, correlations between the physico-chemical properties and the adsorption
116 capacity of MS-13X pellets activated by different methods are discussed. To the best of our knowledge,
117 this is the first work which investigates the use of NTP discharge for both the activation and *in-situ*
118 regeneration of adsorbents and the effect of NTP discharge on the surface and bulk physicochemical
119 properties of adsorbents.

120

121 2. Experimental methods

122.1 Experimental set-up

123 The general schematic representation of the experimental set-up used for the activation of MS-
124 13X and the CSD process is shown in Figure S1. The experimental set-up comprises a gas supply
125 system, MS-13X pellets and glass beads packed bed DBD reactor (shown in Figure S2) and analytical
126 instrumentation for flue gas analysis. The detailed description of the experimental set-up is given in the
127 supplementary information and elsewhere [26].

128.2 Activation of MS-13X

129 To remove the adsorbed carbonaceous compounds and moisture, the purchased MS-13X pellets
130 is usually heated to high temperatures prior to adsorption [27]. In this work, MS-13X pellets was
131 activated using two different methods: (i) by heating and (ii) by NTP exposure. Thermal activation was
132 carried out by heating MS-13X in a flow of dry air (0.2 L min^{-1}) from room temperature to 400°C at a
133 heating rate of 1°C/min and maintained at 400°C for 4 hours [28]. NTP activation was carried out in the
134 DBD reactor using a fixed flow of dry air of 0.5 L min^{-1} for 1 hour using different discharge powers
135 (between 6 and 65 W). The MS-13X samples activated by heating and NTP are labelled as “thermal
136 activated” and “NTP activated”, respectively.

137

1382.3 Cycled storage and discharge process

139 A schematic representation of the different steps in a CSD for the abatement of toluene in dry air
140 is reported elsewhere [9]. The three steps of each cycle of CSD are: (i) the adsorption of toluene on
141 activated MS-13X pellets either until saturation or until a certain critical concentration of toluene is
142 reached, (ii) the desorption of reversibly adsorbed toluene by flushing with dry air and (iii) NTP
143 exposure for the oxidation of irreversibly adsorbed toluene and the regeneration of MS-13X for the next
144 cycle of adsorption. The experimental parameters used during the different steps of the CSD process for
145 the abatement of toluene are summarized in Table S2.

146 The MS-13X samples activated by heating and NTP are labelled as “thermal activated” and “NTP
147 activated”, respectively. The NTP regenerated MS-13X is labelled as “NTP (X) regenerated”, where X
148 corresponds to the number of exposure times to the NTP discharge in addition to the activation (in case
149 of NTP activation).

1502.4 Catalyst characterization

151 The fresh, thermal activated, NTP activated and NTP (II) regenerated MS-13X samples were
152 characterized using different techniques including powder X-ray diffraction (PXRD), X-ray
153 photoelectron spectroscopy (XPS), nitrogen adsorption-desorption analysis, argon sorption and
154 pyridine-Fourier transform infrared spectroscopy (py-FTIR) [29].

1552.5 Stability tests

156 To examine the stability of the zeolite used in this work, 1000 ppm of toluene in dry air (flow rate
157 = 0.1 L/min) was first adsorbed on NTP activated MS-13X until the concentration of toluene in the
158 outlet of the plasma reactor was 10% of the initial concentration. After flushing with dry air, the NTP
159 was turned on for 60 minutes to oxidize the irreversibly adsorbed toluene and to regenerate the MS-
160 13X. This sequence of CSD was repeated for 10 cycles. In addition, the regeneration efficiency (RE)
161 defined as the ratio of the adsorption capacity of the NTP regenerated MS-13X ($[Toluene]_{adsorbed,reg}$)
162 to that of the fresh NTP activated MS-13X ($[Toluene]_{adsorbed,fresh}$) was also calculated.

163

164

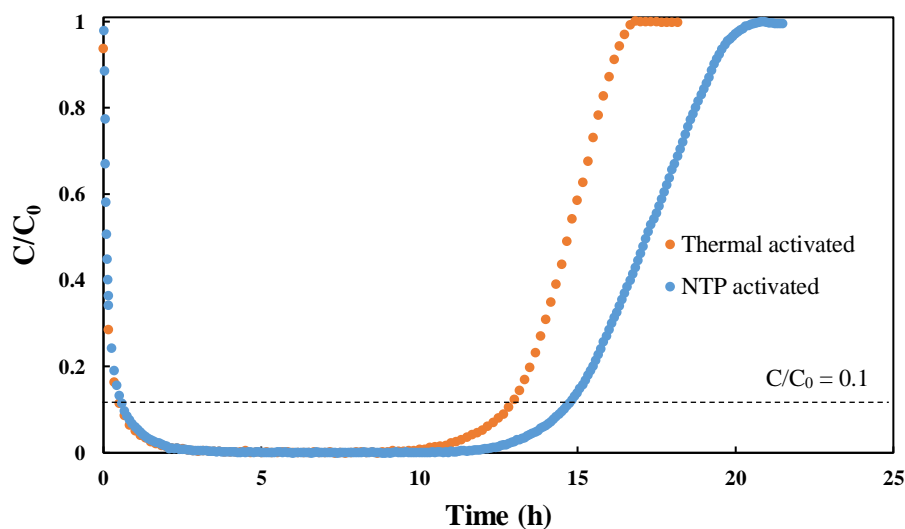
1653. Results and Discussion

1663.1 Activation of 13X zeolite

167 The breakthrough curves of toluene adsorbed on thermal and NTP activated MS-13X are shown
168 in Figure 1 and the amount of adsorbed toluene is determined to be 2.19 ± 0.06 and 2.45 ± 0.06 mmol/g,
169 respectively. These results reveal that the amount of toluene adsorbed on NTP activated MS-13X is
170 ~10% higher than on thermal activated MS-13X. In addition, the time required to reach the critical
171 concentration of toluene in the outlet of the NTP reactor is delayed by 1 hour and 45 minutes for the
172 NTP activated MS-13X. Moreover, the NTP activation of MS-13X is energy efficient as the power
173 consumption of the NTP activation is at least five times lower than the thermal activation.

174 During thermal activation, the main products desorbed from the MS-13X are H₂O and CO₂,
175 whereas during NTP activation, CO₂, H₂O and N₂O are the main products observed. In NTP activation,
176 the adsorbed carbonaceous compounds are desorbed as CO₂ from MS-13X pores either by the reaction
177 with diffused short-lived [30] or long-lived species such as O₃ and N₂O formed in NTP discharge and
178 the adsorbed moisture is desorbed by electropolarization [31]. The amounts of CO₂ desorbed during
179 thermal activation and NTP activation using different applied voltages, shown in Table 1, suggest that
180 the amount of CO₂ desorbed during activation is proportional to the amount of toluene adsorbed on MS-
181 13X. The NTP activation of the MS-13X is performed *in-situ*, whereas the thermal activation is
182 performed *ex-situ* and transferred to the NTP reactor for toluene adsorption. It has been widely reported
183 in literature that 13X zeolite is an efficient adsorbent material for CO₂ owing to its higher pore volume
184 and suitable pore diameter [32] and its low Si/Al ratio with a cation which exhibits strong electrostatic
185 attraction for CO₂ [33]. Thus, the reason for the higher adsorption of toluene from dry air on NTP
186 activated MS-13X using applied voltages ≥ 7.00 kV could be as follows: (i) the amount of CO₂ desorbed
187 by thermal activation is lower than by NTP activation at applied voltages ≥ 7.00 kV (see Table 1) and
188 (ii) adsorption of CO₂ from the atmosphere can occur on the thermal activated sample as it was
189 transferred to the NTP reactor. Thus, in order to investigate the above-mentioned possibilities, the
190 thermal activated sample was also exposed to the NTP. During NTP exposure, more CO₂ and H₂O were
191 desorbed, which can explain the reduced toluene adsorption on the only thermal activated MS-13X.

192 Thus, NTP activation of MS-13X pellets is more efficient in the removal of adsorbed carbonaceous
 193 compounds and moisture and in addition, it eliminates an extra step of sample transfer.



194
 195 *Figure 1 Adsorption of toluene in dry air (initial concentration=1000 ppm; total flow rate=0.1 L/min)*
 196 *on thermal activated and NTP activated MS-13X (applied voltage=7.25 kV; discharge power=58 W;*
 197 *plasma exposure time=1h)*

198
 199 *Table 1 Amount of CO₂ desorbed during activation of MS-13X, amount of toluene adsorbed on*
 200 *activated MS-13X and time to reach the critical concentration of toluene in the outlet of the reactor*
 201 *during adsorption for thermal activated and NTP activated MS-13X (plasma exposure time=1 h)*

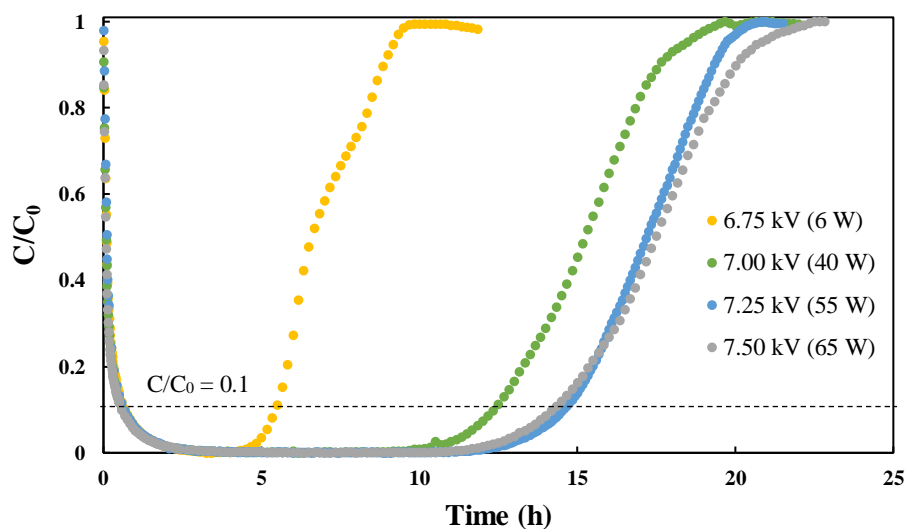
	Applied voltage (kV)	Discharge power (W)	[CO ₂] _{desorbed} (10 th min) (ppm)	[CO ₂] _{total} desorbed (mmol/g)	[Toluene] _{total} adsorbed (mmol/g)	T _{critical} conc (h)
Thermal activated	NA	NA	NA	0.09	2.19 ± 0.06	12.8
	6.75	6	43	0.07	0.93 ± 0.03	5.5
NTP activated	7.00	39	97	0.10	2.22 ± 0.12	12.5

7.25	58	192	0.15	2.45 ± 0.06	14.6
7.50	65	498	0.14	2.46 ± 0.09	14.3

202

203 The FTIR spectra of the outlet gas after 10 minutes of NTP exposure for various applied voltages
204 are shown in Figure S3, in order to visualize the effect of the applied voltage on the amount of CO₂
205 desorbed at a given time. The amount of desorbed CO₂ after 10 minutes increases upon increasing the
206 applied voltage (Table 1 and Figure S3). When the applied voltage increases, the discharge power
207 increases and thus, the energy deposited on MS-13X increases resulting in more desorbed CO₂ after 10
208 minutes of NTP exposure.

209 To further investigate the effect of the applied voltage on the activation of MS-13X, the toluene
210 adsorption capacity of NTP activated MS-13X using different applied voltages was also studied and the
211 breakthrough curves are shown in Figure 2. The amount of toluene adsorbed (mmol/g) and the time
212 required to reach the critical concentration of toluene in the outlet of the NTP reactor are shown in Table
213 1, follow the same trend as that of the total amount of CO₂ desorbed from the MS-13X during NTP
214 activation. Considering that a lower discharge power (58 W) used for activation of MS-13X results in a
215 similar toluene adsorption capacity (approximately 2.45 mmol/g), MS-13X activated by NTP during 1
216 h at an applied voltage of 7.25 kV will be used further on in this study for the investigation of CSD for
217 the removal of toluene.

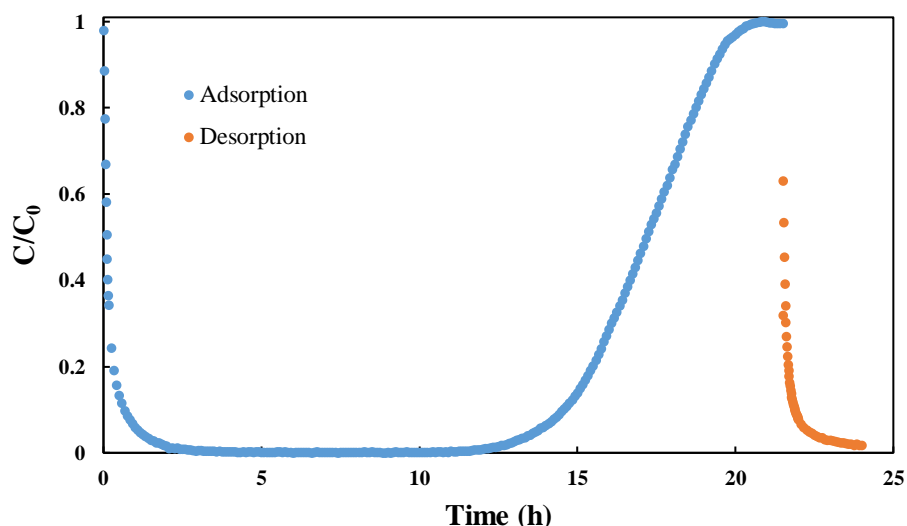


218
 219 *Figure 2 Effect of the applied voltage (and discharge power) during plasma activation on the adsorption*
 220 *of toluene from dry air on NTP activated MS-13X (flow rate=0.1 L/min; initial toluene*
 221 *concentration=1000 ppm; plasma exposure time=1 h)*

2223.2 Cycled storage and discharge process

2231 Adsorption/desorption of toluene on NTP activated MS-13X

224 The breakthrough curve of toluene adsorbed on NTP activated MS-13X at 7.25 kV followed by
 225 the desorption of reversibly adsorbed toluene by flushing dry air is shown in Figure 3. The amount of
 226 toluene adsorbed and the amount of toluene which is reversibly adsorbed on the MS-13X sample are
 227 quantified to be 2.45 ± 0.06 mmol/g and 0.12 mmol/g, respectively. Thus, after flushing with dry air at
 228 room temperature 2.33 ± 0.05 mmol/g of toluene is still adsorbed on the surface of the NTP activated
 229 MS-13X.



230

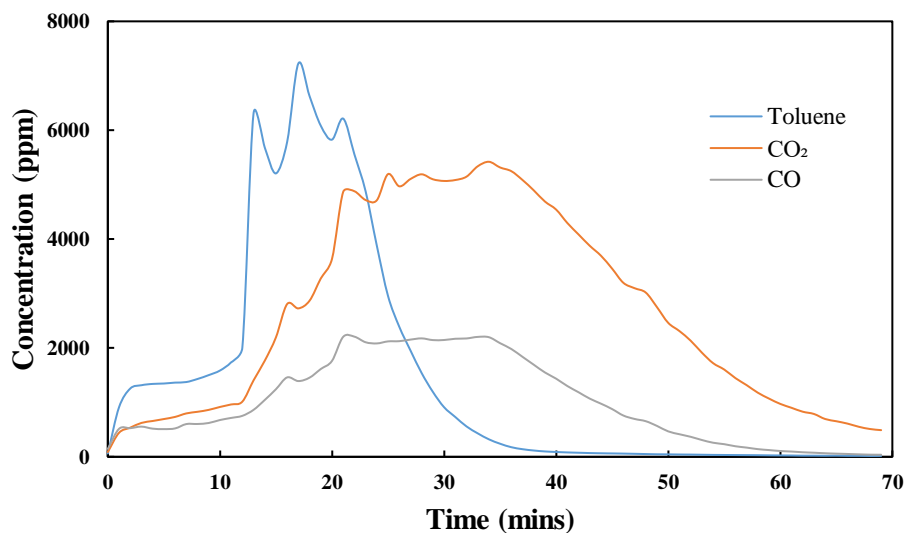
231 *Figure 3 Adsorption of toluene in dry air (initial concentration=1000 ppm; total flow rate=0.1 L/min)*
 232 *and desorption of reversibly adsorbed toluene by dry air flushing (total flow rate=0.5 L/min) on NTP*
 233 *activated MS-13X*

234 **Oxidation of toluene adsorbed on NTP activated MS-13X**

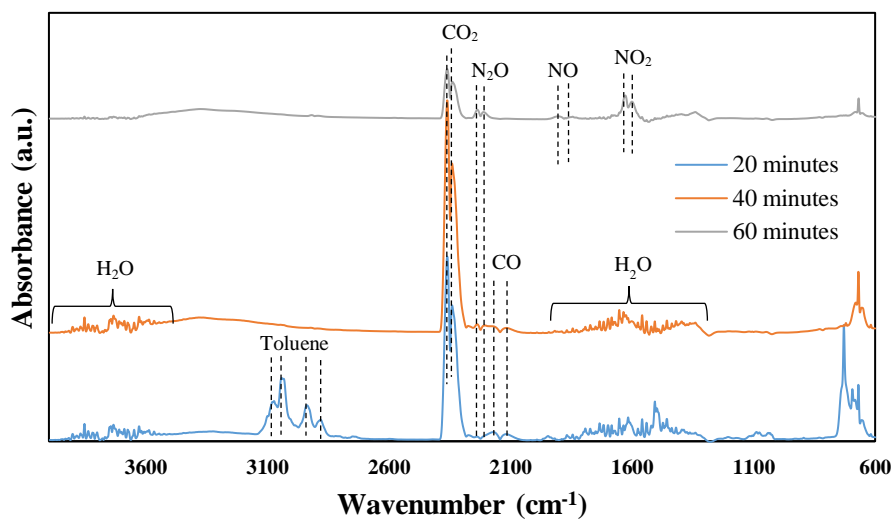
235 During the first 10-30 minutes of NTP exposure, as shown in Figure 4, a significant amount of
 236 the irreversibly adsorbed toluene is desorbed. The total amount of toluene desorbed during this period
 237 is 1.04 mmol/g which accounts for 44.6 % of the irreversibly adsorbed toluene after flushing with dry
 238 air. The toluene desorption by NTP discharge can be reduced by process optimization as follows: (i)
 239 optimizing the NTP operating parameters to reduce the amount of toluene desorbed at a given time and
 240 to increase ozone formation, (ii) optimizing the NTP reactor for ozone generation required for the deep
 241 oxidation of adsorbed toluene, and (iii) subsequent selective adsorption of desorbed unconverted toluene
 242 and conversion. The remaining 1.29 ± 0.03 mmol/g of toluene is converted during NTP exposure. The
 243 two main carbon containing gaseous by-products detected during NTP exposure are CO₂ and CO. As
 244 shown in Figure 4, the concentrations of CO and CO₂ start to increase steeply after 10 minutes of NTP
 245 exposure reaching a plateau after 20 minutes. After approximately 35 minutes of NTP exposure, the
 246 concentrations of CO₂ and CO start to decrease indicating a decrease in the amount of adsorbed toluene
 247 oxidized on the MS-13X surface. The total amount of CO₂ and CO formed are 1.90 mmol/g and 0.72
 248 mmol/g, respectively, which result in a CO₂ and CO selectivity of 21.0 ± 0.4 % and 8.0 ± 0.2 %,
 249 respectively.

250 The FTIR spectra of the outlet gas during NTP treatment at three different exposure times (20,
251 40, and 60 minutes) are shown in Figure 5. Apart from the desorption of unconverted toluene and the
252 formation of CO₂, CO and H₂O, there was also the formation of N₂O (Reaction 12) [34], at 40 and 60
253 minutes and the temporal evolution of N₂O is depicted in Figure 6(a). In addition, the formation of NO
254 and NO₂ was also observed at 60 minutes of NTP exposure. In the temporal evolution of NO (shown in
255 Figure 6(b)), NO is already formed after 40 minutes of NTP exposure. However, this NO formation is
256 not visible in the FTIR spectrum due to the presence of a broad H₂O band which overlaps with the
257 characteristic peaks of NO. The formation of NO is according to the Reaction 13 or the Reaction 14
258 [35], while NO₂ is formed through the oxidation of NO (Reactions 15 & 16) [36]. The increase in the
259 concentration of N₂O and the presence of more electronically excited oxygen atoms result in the
260 formation of NO after 40 minutes of NTP exposure. The formation of NO₂ after 50 minutes of NTP
261 exposure is probably due to the availability of the atomic oxygen species and ozone, which were initially
262 involved in the conversion of adsorbed toluene. As CSD provides the flexibility for the choice of
263 discharge gas and considering the toxicity and negative environmental impact of oxides of nitrogen [37],
264 the formation of these compounds can be avoided by using non-nitrogen gas such as O₂ diluted in He or
265 Ar during the discharge stage. Ozone, which is one of the main oxygen species produced in a dry air
266 plasma [26] was also detected in the outlet of the MS-13X pellets & glass beads packed bed DBD
267 reactor, but only during the first 5 minutes of NTP exposure. The temporal evolution of O₃ (not shown
268 here) showed an initial O₃ concentration of 200 ppm immediately after plasma ignition, which rapidly
269 decreased to zero after five minutes of NTP exposure.

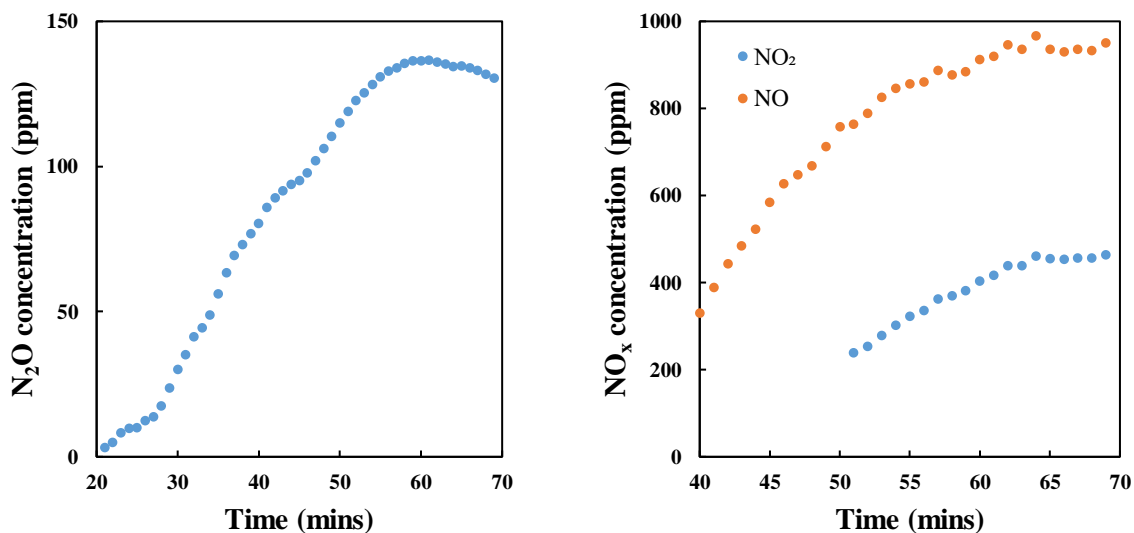




275
 276 *Figure 4 Temporal evolution of the concentration of desorbed toluene, CO₂ and CO formed during NTP*
 277 *exposure at the plasma reactor outlet (total flow rate=0.5 L/min; applied voltage=7.5 kV; discharge*
 278 *power=65 W)*



279
 280 *Figure 5 FTIR spectra of the plasma reactor outlet gas during NTP exposure of NTP activated MS-13X*
 281 *at three different times after NTP ignition (20, 40 and 60 minutes) (total flow rate=0.5 L/min; applied*
 282 *voltage=7.5 kV; discharge power=65 W)*



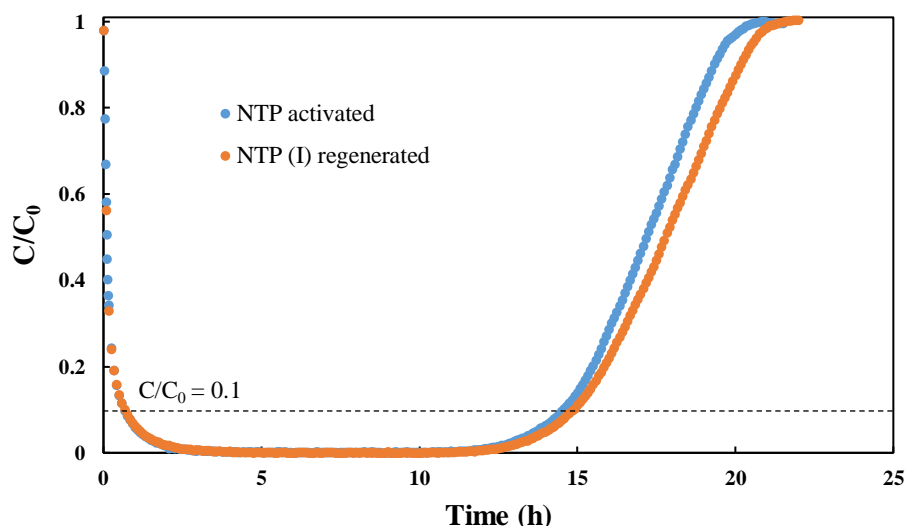
283 *Figure 6 Temporal evolution of the concentration of different nitrogen containing by-products: (a) N₂O,*
 284 *(b) NO and NO₂ during NTP exposure of NTP activated MS-13X*

285

286 2.6.3 Regeneration of 13X zeolite

287 The breakthrough curves of toluene adsorbed on NTP activated (fresh) and NTP (I) regenerated
 288 (used) MS-13X are shown in Figure 7. From Figure 7, it is determined that the total amount of toluene
 289 adsorbed on NTP (I) regenerated MS-13X is 2.49 ± 0.03 mmol/g, which is similar to that of the fresh
 290 NTP activated MS-13X. The critical concentration of toluene was also observed after 14.6 and 14.9
 291 hours for NTP activated and NTP (I) regenerated MS-13X, respectively. These results demonstrate the
 292 complete regeneration of the used MS-13X after one cycle of CSD.

293

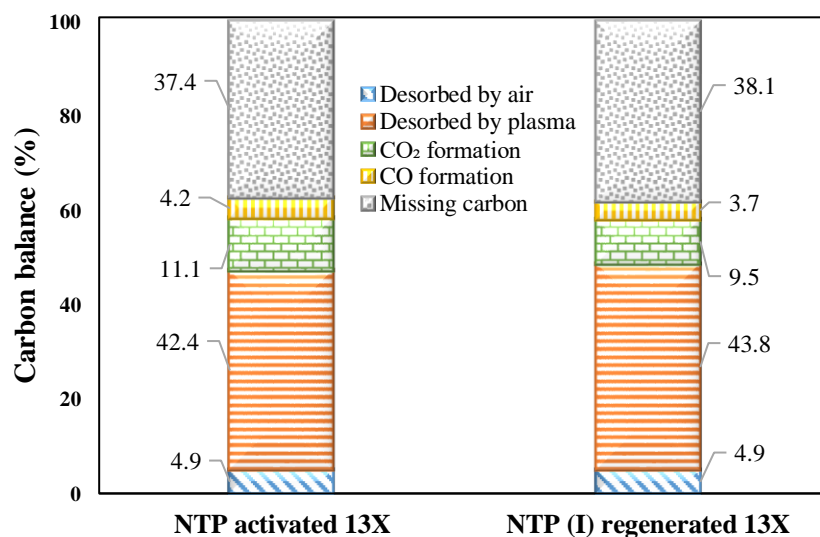


294

295 *Figure 7 Breakthrough curves for the adsorption of toluene from dry air until saturation on NTP*
 296 *activated and NTP (I) regenerated MS-13X*

297 In this work, the carbon balances were calculated by considering the total amount of toluene
 298 adsorbed as 100%. As shown in Figure 8 and Table S3, the amounts of toluene desorbed by the flushing
 299 of dry air for NTP activated and NTP (I) regenerated MS-13X are the same. On the other hand, the
 300 desorption of unconverted toluene by the NTP discharge for the NTP (I) regenerated MS-13X (43.8%)
 301 sample is slightly higher than the NTP activated MS-13X sample (42.4%), resulting in the same amount
 302 of toluene converted for both samples. Finally, the CO_x yield of the NTP (I) regenerated sample is lower
 303 than the NTP activated MS-13X, resulting in slightly more missing carbon for the former sample. The
 304 missing carbon for both zeolite samples could be explained by the presence of oil-like deposits on the
 305 inner wall of the plasma reactor outside the plasma discharge zone, which was also reported by other
 306 researchers even in the presence of transition metal oxide catalysts [38]. The formation of these deposits
 307 could be potentially reduced by heating the walls of the plasma reactor, by increasing the applied gas
 308 flow rate and by loading transition metal oxide on MS-13X [39]. To conclude, for the same amount of
 309 converted toluene, more CO₂ and CO are formed when using the NTP activated MS-13X compared to
 310 the NTP (I) regenerated MS-13X, consequently resulting in a higher CO₂ and CO selectivity for NTP
 311 activated MS-13X. On the other hand, the higher adsorption time on the NTP (I) regenerated MS-13X
 312 results in a lower energy cost to remedy 1 m³ of air (Table 2), whereas the energy yield remains the

313 same for both the MS-13X. The performance of APC/CSD process using MS-13X reported in various
 314 work are listed in Table 3. This overview highlights that comparable CO_x yield has been obtained in this
 315 work despite higher amount of toluene adsorbed on MS-13X and suggests that metal loading on MS-
 316 13X yields better selectivity towards CO₂ formation.



317

318 *Figure 8 Carbon balance of the NTP activated and NTP (I) regenerated MS-13X*

319

320 *Table 2 CO_x yield, product selectivity, energy cost and energy yield for NTP activated and NTP (I)*
 321 *regenerated MS-13X*

	NTP activated	NTP (I) regenerated
	MS-13X	
CO _x yield (%)	15.3 ± 0.3	13.2 ± 0.2
CO ₂ selectivity (%)	21.0 ± 0.4	18.5 ± 0.2
CO selectivity (%)	8.0 ± 0.2	7.1 ± 0.1
CO _x selectivity (%)	29.0 ± 0.6	25.7 ± 0.3

Energy cost (kWhm ⁻³)	0.60	0.55
Energy yield (g/kWh)	6.04 ± 0.13	6.13 ± 0.07

322

323 *Table 3 Overview of reported work on toluene abatement by APC/CSD process using MS-13X*

Adsorbent	Toluene adsorbed (mmol)	NTP reactor	Discharge gas	CO _x yield (%)	Regeneration	Ref.
MS-13X	2.45	DBD (ventilated)	Air	15	Yes	This work
MS-13X	0.57	DBD (ventilated)	Air	20	n.a.	[18]
MS-13X	0.57	DBD (closed)	Air	<5	n.a.	[19]
Co/MS- 13X	0.51	DBD (ventilated)	Air	80	n.a.	[19]
Co/MS- 13X	0.51	DBD (ventilated)	O ₂	100	n.a.	[19]

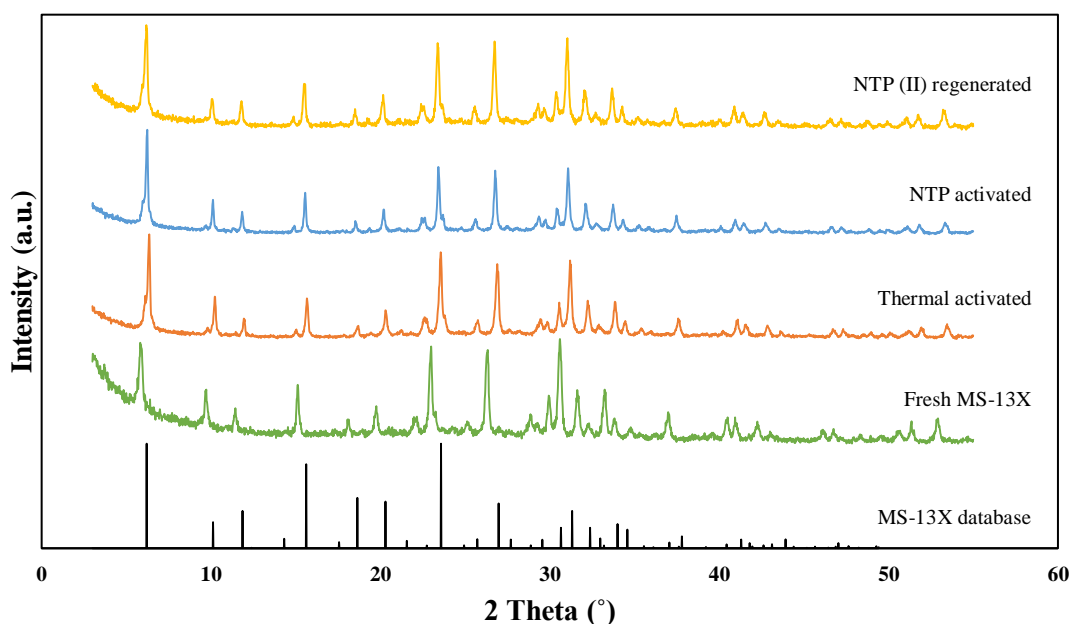
324

3253.3 Surface and bulk properties of activated and regenerated MS-13X

326 The surface and bulk properties of the thermal activated, NTP activated and NTP regenerated
 327 MS-13X are investigated in this section. To understand the effect of NTP exposure on the MS-13X
 328 properties and to establish correlations between the properties and its performance in APC process, the
 329 surface and bulk properties of the zeolite are measured.

330 As a first step, the PXRD patterns of the fresh, thermal activated, NTP activated and NTP (II)
 331 regenerated MS-13X are studied to examine the crystallinity of the samples after plasma exposure
 332 (shown in Figure 9). The fresh MS-13X sample is regarded as the reference sample for this particular

333 study. The diffraction of the three samples match with those reported for the FAU structure of MS-13X
334 (JCPDS card No. 38-0237) by other researchers [40–44]. Moreover, no shift in the diffractions and no
335 significant diffraction lines corresponding to any new phase is observed after NTP exposure. This
336 observation, together with the remaining high diffraction intensities and low background, clearly show
337 that the crystallinity of MS-13X is maintained.



338
339 Figure 9 PXRD patterns of fresh, thermal activated, NTP activated and NTP (II) regenerated MS-13X

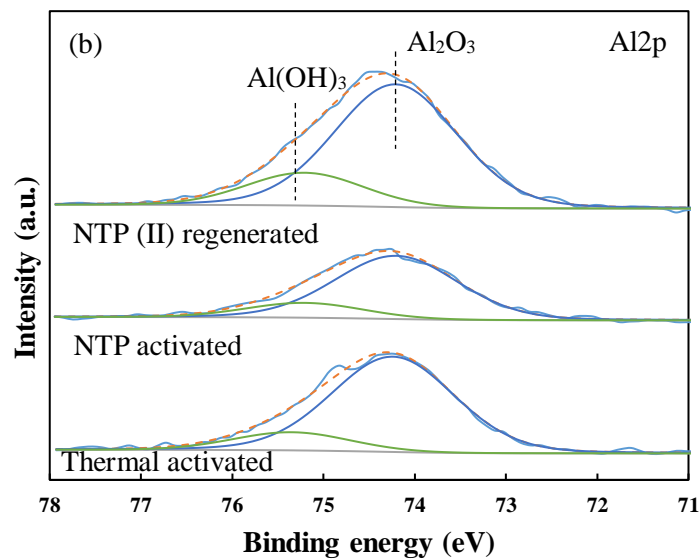
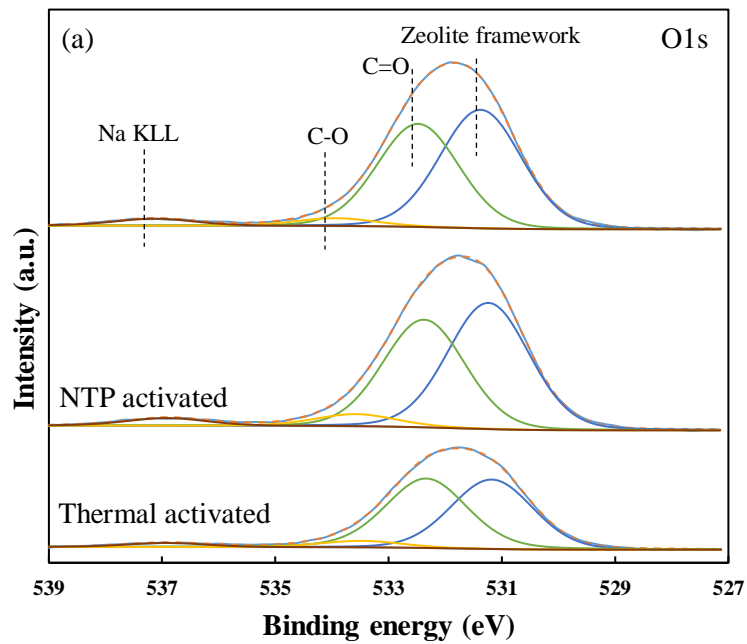
340 The XPS survey spectra of the thermal activated, NTP activated and NTP (II) regenerated MS-
341 13X reveal the presence of the following elements: C, O, Na, Si, Al and Ca and the corresponding
342 surface elemental composition is shown in Table 4. This analysis reveals that the examined zeolite
343 samples have a similar surface elemental composition. It is known from literature that the adsorption
344 capacity of zeolites changes as a function of their Si/Al ratio [45]. However, there is no difference in
345 the surface Si/Al ratio of thermal and NTP activated MS-13X samples.

346 The high-resolution O1s & Al2p and C1s, Na1s & Si2p spectra of the thermal activated, NTP
347 activated and NTP (II) regenerated MS-13X are shown in Figure 10 and Figure S4 respectively. The
348 high-resolution C1s (either impurities or adsorbed carbonaceous compounds) spectra (Figure S4(a)) are
349 deconvoluted into four photopeaks centred at 285.0, 286.4, 287.5 and 289.2 eV, which correspond to C-
350 C, C-O, C=O and O-C=O bonds, respectively [46]. No significant differences are observed in the relative

351 areas of these peaks for the three investigated zeolite samples suggesting that there is no deposition of
352 carbon containing compounds (see Figure 8) from the CSD process. The high-resolution O1s region
353 (shown in Figure 10(a)) are deconvoluted by using 4 photopeaks centred at 531.2, 532.3, 533.4 and 537
354 eV. The first photopeak at 531.2 eV corresponds to the oxygen present in the zeolite framework, whereas
355 the photopeaks at 532.3 and 533.4 eV correspond to C=O and O=C-O bonds and the photopeak at 537
356 eV corresponds to Na KLL [47]. From the depicted O1s spectra, it can be seen that the oxygen
357 percentage in the zeolite framework for the NTP activated (49.6 %) and the NTP (II) regenerated (50.0
358 %) MS-13X is higher than in case of the thermal activated MS-13X (45.0 %). This observation suggests
359 that NTP activation of MS-13X desorbs the carbonaceous compounds (especially CO₂) more effectively.
360 In addition, the ratio of the oxygen present in the zeolite framework (531.2 eV) to the adsorbed oxygen
361 (532.3 and 533.4 eV) for NTP activated (1.05) and NTP (II) regenerated (1.06) MS-13X is similar,
362 suggesting that there are no residual carbon containing compounds in the MS-13X after 2 cycles of CSD.
363 Figure S4(b) depicts the Na1s spectra of the examined zeolites. In all samples, only one broad photopeak
364 was observed at ~ 1072 eV, which can be assigned to Na₂O [48]. No shift in the Na1s peak of MS-13X
365 was observed for any of the samples shows that the ionicity of the Na-O bonds was maintained after
366 NTP exposure [49]. Figure S4(c) shows the high-resolution Si2p spectra of all the samples. These
367 spectra are deconvoluted using 2 different peaks, which are centred at 103.4 eV and 102.4. The former
368 peak can be attributed to the Si-O bonds in SiO₂, while the latter can be assigned to silicates. Moreover,
369 there is no shift in the peak position of the Si-O bonds at 102.4 eV, suggesting that there is no change in
370 the covalent nature of this bond due to plasma activation or cyclic CSD process [50]. In addition, there
371 is also no shift in the peak which corresponds to silicates (peak centred at 103.4 eV). Finally, Figure
372 10(b) shows the Al2p spectra, which are deconvoluted using two peaks centred at 74.2 eV and 75.2 eV,
373 that correspond to the Al-O bonds of Al₂O₃ and Al(OH)₃, respectively. From the Al2p spectra, the
374 relative area of the peak centred at 75.2 eV (attributed to Al(OH)₃) in the NTP activated (18 %) and the
375 NTP (II) regenerated (19 %) zeolite are similar to that of the thermal activated (16 %) MS-13X, which
376 shows that there is no change in the presence of the EFAL species in MS-13X after NTP exposure.

Table 4 Surface elemental composition obtained from XPS survey spectra for thermal activated, NTP activated and NTP (II) regenerated MS-13X

	Atomic percentage (%)						
	C	O	Na	Al	Si	Ca	Si/Al
Thermal activated	9.0 ± 0.8	61.8 ± 0.4	6.4 ± 0.3	6.3 ± 0.0	15.6 ± 0.7	0.9 ± 0.1	2.5
NTP activated	9.4 ± 0.8	60.6 ± 1.1	6.3 ± 0.6	6.4 ± 0.6	15.7 ± 0.5	1.3 ± 0.1	2.4
NTP (II) regenerated	8.9 ± 0.6	61.7 ± 0.8	5.9 ± 0.2	6.3 ± 0.6	16.0 ± 0.4	1.2 ± 0.1	2.5



382 *Figure 10 XPS high-resolution spectra of (a) O1s and (b) Al2p for thermal activated, NTP activated*
 383 *and NTP (II) regenerated MS-13X*

384 The nitrogen adsorption-desorption isotherms of the fresh, thermal activated, NTP activated and
 385 NTP (II) regenerated MS-13X are shown in Figure S5(a). The isotherms of all samples belong to the
 386 type IV, in accordance with the IUPAC classification. At low relative pressure ($P/P_0 < 0.01$), the
 387 adsorbed volume sharply increases, after which a constant adsorbed volume in the relative pressure

388 range of 0.1-0.6 is observed. The first increase is attributed to the filling of the micropores, whereas the
 389 second increase is visible at a relative pressure close to 1.0, which is probably due to the presence of
 390 macropores resulting from the use of binders and pore forming agents in the pelletization process. The
 391 specific surface area S_{BET} and pore volume of the four MS-13X samples are shown in Table 5. The
 392 results show that the S_{BET} of activated MS-13X is higher than the fresh MS-13X and there are no
 393 significant changes in the S_{BET} and pore volume after one-time (NTP activated) and three-times (NTP
 394 (II) regenerated) NTP exposure. The BJH (Barrett-Joyner-Halenda) pore size distribution (PSD) (Figure
 395 S5(b)) shows a broad distribution of mesopores (between 2 nm and 50 nm) for all samples. Additionally,
 396 there are no significant differences in PSD for the examined zeolites.

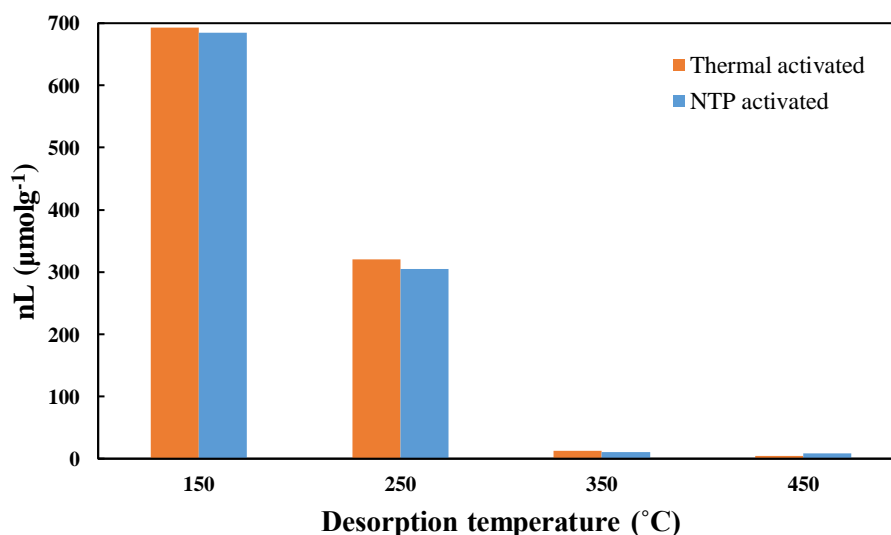
397 Although N_2 adsorption-desorption analysis is widely used to determine the surface properties, it
 398 is not suitable for the investigation of micropores in zeolites [51]. Thus, Ar was also used as an adsorbate
 399 for the analysis of the micropores in thermal and NTP activated MS-13X samples. The obtained Ar
 400 adsorption isotherms and the corresponding PSD are shown in Figure S6. The specific surface area
 401 (S_{BET}) of the NTP activated MS-13X is slightly lower in comparison to the thermal activated MS-13X
 402 (Table 5). The PSDs depicted in Figure S6(b) reveal a narrow distribution of micropores with a
 403 maximum around 1 nm.

404 *Table 5 Surface properties of fresh, thermal activated, NTP activated and NTP regenerated MS-13X*

	Fresh	Thermal activated	NTP activated	NTP (II) regenerated
S_{BET} (m^2/g) – N_2 sorption	312	347	352	347
Pore volume (ml/g) – N_2 sorption	0.10	0.24	0.24	0.24
S_{BET} (m^2/g) – Ar sorption	--	569	521	--

405
 406 In order to investigate the effect of NTP exposure on the migration of aluminium from the
 407 framework, resulting in extra framework aluminium (EFAI), which are Lewis acid sites [52,53], *in-situ*
 408 IR spectroscopy of pyridine adsorbed on thermal and NTP activated MS-13X was performed. In

409 addition, the analysis of the IR spectra of the OH groups were investigated to get more information
410 about the nature of the acid sites. Figure S7(a) and (b) show the IR bands in the region 1570 – 1400 cm⁻¹
411 ¹. The two absorption bands observed in this region correspond to the C-C stretch of coordinatively
412 bonded pyridine indicating the presence of Lewis acid sites (1445 cm⁻¹) and pyridine interacting with
413 both Lewis and Brønsted acid sites (1490 cm⁻¹) [54]. On the other hand, the absorption peak
414 corresponding to the stretching vibration of the pyridinium ion which is used to detect the Brønsted acid
415 sites could not be seen in the obtained FTIR spectra [55,56]. Figure S7 also shows that with increasing
416 the pyridine desorption temperature, the intensity of the bands at 1490 cm⁻¹ and 1445 cm⁻¹ decreases for
417 both zeolites, which proves that mainly weak acidic sites are present in both MS-13X samples. The
418 surface concentration of Lewis acid sites (Figure 11) clearly shows that the type and amount of acid
419 sites is similar on the thermal and NTP activated zeolite for all examined desorption temperatures and
420 there is no change in the amount of Lewis acid sites after NTP exposure. Figure S8 shows the IR bands
421 in the region 3850 – 3550 cm⁻¹ at pyridine desorption temperature of 450 °C. In both the samples, the
422 band around 3740 cm⁻¹ is attributed to surface silanols groups terminating the exterior of the crystal and
423 the band around 3675 cm⁻¹ is attributed to an OH group on EFAI species [57].

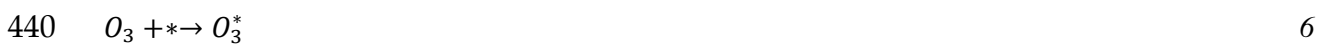


424
425 *Figure 11 Evolution of the amount of Lewis acid sites as a function of the pyridine desorption*
426 *temperature for thermal activated and NTP activated MS-13X*

427
428

4293.4 Reaction mechanism for the oxidation of toluene adsorbed on MS-13X

430 The exact adsorption mechanism of basic VOCs such as toluene on zeolites is still under debate
431 but it has already been reported that toluene can be adsorbed both on the Lewis and Brønsted acid sites
432 [58]. Based on the characterization of the acid sites performed in this study and on the OES
433 measurement in our previous study [26], the plausible reaction mechanism for toluene oxidation is
434 proposed. The adsorption of toluene on MS-13X is dominated by the formation of Lewis acid-base
435 adducts. During NTP exposure, decomposition of adsorbed toluene occurs (i) in the gas phase for the
436 desorbed toluene and (ii) on the surface of the MS-13X for the irreversibly adsorbed toluene. As the
437 reaction mechanism of toluene oxidation in the gas phase is already well explained in literature, the
438 reader is referred to an earlier study [9]. On the other hand, the decomposition of toluene on the surface
439 of MS-13X proceeds by the following reactions:



444 where * represents the surface active sites, O_3^* is ozone adsorbed on the zeolite and O_2^* and O_2 are the
445 surface oxide species. The adsorption and decomposition of ozone on MS-13X (Reactions 17 and 18)
446 are due to the presence of Lewis acid sites [56,60], which was already confirmed by the pyridine FTIR
447 study. Before switching on the NTP, the saturation of the MS-13X with toluene could occupy all
448 available Lewis acid sites, which in turn explains the presence of ozone in the exit of the NTP reactor
449 for the first five minutes of NTP exposure (Section 3.2.2). Afterwards, the desorption of toluene by NTP
450 exposure (see Figure 4) makes some Lewis acid sites available for the adsorption and decomposition of
451 ozone, which generates active oxygen species, which in turn react with adsorbed toluene. This explains
452 the steep increase in the formation of CO_2 and CO after 10 minutes of NTP exposure (see Figure 4) by
453 the following reaction:

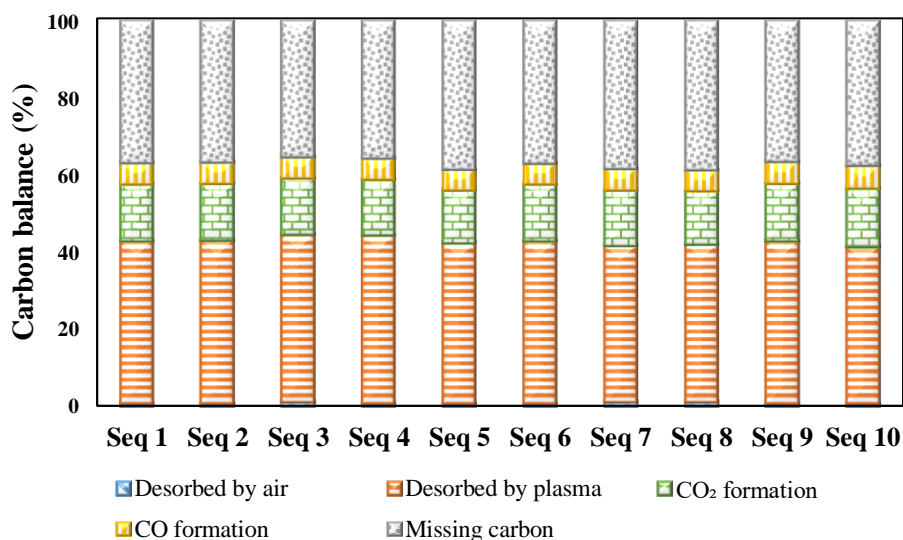


455

456

4573.5 Stability of MS-13X for cyclic adsorption-plasma catalysis

458 In this work, the stability of the NTP activated MS-13X was analyzed by saturating MS-13X until
459 the critical outlet concentration of toluene for 10 cycles of the CSD process. The carbon balance, the
460 total amount of adsorbed toluene, the regeneration efficiency and the product (CO_2 and CO_x) selectivity
461 are shown in Figure 12 and Table S4. The total amount of adsorbed toluene during 10 cycles was in the
462 range 1.8 - 1.9 mmol/g which demonstrates that the NTP exposure completely regenerates the MS-13X.
463 The amount of toluene desorbed by flushing air and the amount of toluene desorbed by NTP exposure
464 was similar for all cycles. The regeneration efficiency is higher than 97% for all 10 cycles (Table S4).
465 In addition, the CO_2 and CO_x selectivities also remain constant at approximately $25.6 \pm 1.0 \%$ and 35.4
466 $\pm 1.4 \%$, respectively. These experimental results suggest that the MS-13X is stable during 10 cycles of
467 NTP exposure, or in other words, the applied CSD technique is a promising process for the removal of
468 toluene from air and the regeneration of the used MS-13X.



469
470 *Figure 12 Carbon balance for the adsorption plasma catalytic abatement of toluene adsorbed until the*
471 *critical concentration on NTP activated and NTP regenerated MS-13X for 10 cycles*

472

4734. Conclusion

474 This work investigates the use of non-thermal plasma for the activation and regeneration of MS-
475 13X pellets during CSD of toluene. The NTP activation of MS-13X by NTP results in a higher toluene

476 adsorption when compared to the thermal activation. Analysis of the surface and bulk properties of
477 thermal activated and NTP activated MS-13X shows that the crystallinity, pore volume, pore size
478 distribution, type and amount of acid sites and elemental composition are not altered by the plasma
479 discharge.

480 The regeneration of MS-13X by NTP exposure is also demonstrated in this study by comparing the
481 amount of adsorbed toluene, and by determining the catalytic activity using fresh NTP activated and
482 used NTP regenerated MS-13X for the CSD removal of toluene. The amount of toluene adsorbed on
483 both MS-13X samples remains unaltered, whereas the CO_x yield is marginally reduced for the NTP
484 regenerated MS-13X. Analysis of the bulk and surface properties of the fresh NTP activated and used
485 NTP regenerated MS-13X reveals no significant difference between both samples, suggesting complete
486 regeneration of the MS-13X by NTP exposure. Finally, a study on the stability and regeneration
487 efficiency of MS-13X by NTP exposure for 10 cycles of CSD removal of toluene shows a complete
488 regeneration of the used MS-13X.

489 This work thus clearly demonstrates that the use of MS-13X for the CSD elimination of toluene
490 fulfils the following criteria: (i) an improved ratio of adsorption time to NTP exposure time, thus a
491 reduced energy cost of the process, (ii) stability of the MS-13X in the discharge and (iii) regenerability
492 of the MS-13X by NTP exposure. Unfortunately, there was no total oxidation of toluene, resulting in
493 missing carbon and CO formation which corresponds to 42% of the total adsorbed carbon, irrespective
494 of the initial amount of adsorbed toluene. This implies that further work has to be done to enhance the
495 total toluene oxidation either by engineering the adsorbent or by process optimization.

496

497 **Acknowledgments**

498 The project "DepollutAir" funded by the European Program INTERREG V France-Wallonie-Flanders
499 FEDER is acknowledged for supporting and funding this research work (grant number 1.1.18). This
500 research was carried out in the French-Belgium Associated International Laboratory "Plasma &
501 Catalysis" supported by the University of Lille and Ghent University.

502

503

- 505 [1] C.O. Baltaretu, E.I. Lichtman, A.B. Hadler, M.J. Elrod, Primary
506 atmospheric oxidation mechanism for toluene, *The Journal of*
507 *Physical Chemistry A*. 113 (2009) 221–230.
508 <https://doi.org/10.1021/jp806841t>.
- 509 [2] F.I. Khan, A. Kr. Ghoshal, Removal of Volatile Organic
510 Compounds from polluted air, *Journal of Loss Prevention in the*
511 *Process Industries*. 13 (2000) 527–545.
512 [https://doi.org/10.1016/S0950-4230\(00\)00007-3](https://doi.org/10.1016/S0950-4230(00)00007-3).
- 513 [3] A.M. Vandebroucke, R. Morent, N. De Geyter, C. Leys, Non-
514 thermal plasmas for non-catalytic and catalytic VOC abatement, *J*
515 *Hazard Mater*. 195 (2011) 30–54.
516 <https://doi.org/10.1016/j.jhazmat.2011.08.060>.
- 517 [4] F. Gironi, V. Piemonte, VOCs removal from dilute vapour streams
518 by adsorption onto activated carbon, *Chemical Engineering*
519 *Journal*. 172 (2011) 671–677.
520 <https://doi.org/10.1016/j.cej.2011.06.034>.
- 521 [5] F. Salvador, N. Martin-Sanchez, R. Sanchez-Hernandez, M.J.
522 Sanchez-Montero, C. Izquierdo, Regeneration of carbonaceous
523 adsorbents. Part II: Chemical, Microbiological and Vacuum
524 Regeneration, *Microporous and Mesoporous Materials*. 202 (2015)
525 277–296. <https://doi.org/10.1016/j.micromeso.2014.08.019>.
- 526 [6] F. Salvador, N. Martin-Sanchez, R. Sanchez-Hernandez, M.J.
527 Sanchez-Montero, C. Izquierdo, Regeneration of carbonaceous
528 adsorbents. Part I: Thermal Regeneration, *Microporous and*
529 *Mesoporous Materials*. 202 (2015) 259–276.
530 <https://doi.org/10.1016/j.micromeso.2014.02.045>.
- 531 [7] K.-J. Kim, H.-G. Ahn, The effect of pore structure of zeolite on the
532 adsorption of VOCs and their desorption properties by microwave
533 heating, *Microporous and Mesoporous Materials*. 152 (2012) 78–
534 83. <https://doi.org/10.1016/j.micromesa.2011.11.051>.
- 535 [8] Z.-Z. Xie, L. Wang, G. Cheng, L. Shi, Y.-B. Zhang, Adsorption
536 properties of regenerative materials for removal of low
537 concentration of toluene, *J Air Waste Manage Assoc*. 66 (2016)
538 1224–1236. <https://doi.org/10.1080/10962247.2016.1209257>.
- 539 [9] S.K.P. Veerapandian, J.-M. Giraudon, N. De Geyter, Y.
540 Onyshchenko, C. Krishnaraj, S. Sonar, A. Löfberg, K. Leus, P. Van
541 Der Voort, J.-F. Lamonier, R. Morent, Regeneration of Hopcalite
542 used for the adsorption plasma catalytic removal of toluene by non-
543 thermal plasma, *Journal of Hazardous Materials*. (2020) 123877.
544 <https://doi.org/10.1016/j.jhazmat.2020.123877>.
- 545 [10] L.Y. Jia, A. Farouha, L. Pinard, S. Hedan, J.D. Comparot, A.
546 Dufour, K. Ben Tayeb, H. Vezin, C. Batiot-Dupeyrat, New routes
547 for complete regeneration of coked zeolite, *Applied Catalysis B:*
548 *Environmental*. 219 (2017) 82–91.
549 <https://doi.org/10.1016/j.apcatb.2017.07.040>.
- 550 [11] S.K.P. Veerapandian, N. De Geyter, J.M. Giraudon, J.F. Lamonier,
551 R. Morent, The use of zeolites for VOCs abatement by combining
552 non-thermal plasma, adsorption, and/or catalysis: A review,
553 *Catalysts*. 9 (2019). <https://doi.org/10.3390/catal9010098>.
- 554 [12] E. Van Bavel, V. Meynen, P. Cool, K. Lebeau, E.F. Vansant,
555 Adsorption of hydrocarbons on mesoporous SBA-15 and PHTS
556 materials, *Langmuir*. 21 (2005) 2447–2453.
557 <https://doi.org/10.1021/la0474417>.

558
559
560
561
562
563
564
565
566
567
568
569
570
571
572
573
574
575
576
577
578
579
580
581
582
583
584
585
586
587
588
589
590
591
592
593
594
595
596
597
598
599
600
601
602
603
604
605
606
607
608
609
610
611
612

- [13] M. Ghafari, J.D. Atkinson, Impact of styrenic polymer one-step hyper-cross-linking on volatile organic compound adsorption and desorption performance, *Journal of Hazardous Materials*. 351 (2018) 117–123. <https://doi.org/10.1016/j.jhazmat.2018.02.051>.
- [14] F. Noël, C.A. Serra, S. Le Calvé, micromachines Design of a Novel Axial Gas Pulses Micromixer and Simulations of its Mixing Abilities via Computational Fluid Dynamics, (2019). <https://doi.org/10.3390/mi10030205>.
- [15] I. Tsukada, S. Higuchi, Pulsed-laser deposition of LiNbO₃ in low gas pressure using pure ozone e, *Japanese Journal of Applied Physics*. 43 (2004) 5307. <https://doi.org/10.1143/JJAP.43.5307>.
- [16] C.Y.H. Chao, C.W. Kwong, K.S. Hui, Potential use of a combined ozone and zeolite system for gaseous toluene elimination, *Journal of Hazardous Materials*. 143 (2007) 118–127. <https://doi.org/10.1016/j.jhazmat.2006.08.077>.
- [17] J. Van Durme, J. Dewulf, W. Sysmans, C. Leys, H. Van Langenhove, Abatement and degradation pathways of toluene in indoor air by positive corona discharge, *Chemosphere*. 68 (2007) 1821–1829. <https://doi.org/10.1016/j.chemosphere.2007.03.053>.
- [18] H. Yi, X. Yang, X. Tang, S. Zhao, J. Wang, X. Cui, T. Feng, Y. Ma, Removal of toluene from industrial gas over 13X zeolite supported catalysts by adsorption-plasma catalytic process, *Journal of Chemical Technology and Biotechnology*. 92 (2017) 2276–2286. <https://doi.org/10.1002/jctb.5314>.
- [19] H. Yi, X. Yang, X. Tang, S. Zhao, Removal of toluene from industrial gas by adsorption–plasma catalytic process : Comparison of closed discharge and ventilated discharge, *Plasma Chemistry and Plasma Processing*. 38 (2018) 331–345. <https://doi.org/10.1007/s11090-017-9863-1>.
- [20] Q.H. Trinh, S.B. Lee, Y.S. Mok, Removal of ethylene from air stream by adsorption and plasma-catalytic oxidation using silver-based bimetallic catalysts supported on zeolite, *Journal of Hazardous Materials*. 285 (2015) 525–534. <https://doi.org/10.1016/j.jhazmat.2014.12.019>.
- [21] Q.H. Trinh, Y.S. Mok, Effect of the adsorbent/catalyst preparation method and plasma reactor configuration on the removal of dilute ethylene from air stream, *Catalysis Today*. 256 (2015) 170–177. <https://doi.org/10.1016/j.cattod.2015.01.027>.
- [22] H.H. Kim, J.H. Kim, A. Ogata, Adsorption and oxygen plasma-driven catalysis for total oxidation of VOCs, *International Journal of Plasma Environmental Science & Technology*. 2 (2008) 106–112. <https://doi.org/10.34343/ijpest.2008.02.02.106>.
- [23] H.H. Kim, A. Ogata, S. Futamura, Oxygen partial pressure-dependent behavior of various catalysts for the total oxidation of VOCs using cycled system of adsorption and oxygen plasma, *Applied Catalysis B: Environmental*. 79 (2008) 356–367. <https://doi.org/10.1016/j.apcatb.2007.10.038>.
- [24] K. Shang, J. Ren, Q. Zhang, N. Lu, N. Jiang, J. Li, Successive treatment of benzene and derived byproducts by a novel plasma catalysis-adsorption process, *Journal of Environmental Chemical Engineering*. 9 (2021) 105767. <https://doi.org/10.1016/J.JECE.2021.105767>.
- [25] S. Li, X. Yu, X. Dang, P. Wang, X. Meng, Q. Wang, H. Hou, Double dielectric barrier discharge incorporated with CeO₂-Co₃O₄/γ-Al₂O₃ catalyst for toluene abatement by a sequential

- 613 adsorption–discharge plasma catalytic process, *Journal of Cleaner*
614 *Production*. 340 (2022) 130774.
615 <https://doi.org/10.1016/J.JCLEPRO.2022.130774>.
- 616 [26] Z. Ye, S.K.P. Veerapandian, I. Onyshchenko, A. Nikiforov, N. De
617 Geyter, J.-M. Giraudon, J.-F. Lamonier, R. Morent, An in-Depth
618 Investigation of Toluene Decomposition with a Glass Beads-
619 Packed Bed Dielectric Barrier Discharge Reactor, *Industrial and*
620 *Engineering Chemistry Research*. 56 (2017).
621 <https://doi.org/10.1021/acs.iecr.7b00963>.
- 622 [27] G. Swetha, T. Gopi, S. Chandra Shekar, C. Ramakrishna, B. Saini,
623 P.V.L. Rao, Combination of adsorption followed by ozone
624 oxidation with pressure swing adsorption technology for the
625 removal of VOCs from contaminated air streams, *Chemical*
626 *Engineering Research and Design*. 117 (2017) 725–732.
627 <https://doi.org/10.1016/j.cherd.2016.11.036>.
- 628 [28] S. Huang, W. Deng, L. Zhang, D. Yang, Q. Gao, Z. Tian, L. Guo,
629 T. Ishihara, Adsorptive properties in toluene removal over
630 hierarchical zeolites, *Microporous and Mesoporous Materials*. 302
631 (2020) 110204. <https://doi.org/10.1016/j.micromeso.2020.110204>.
- 632 [29] G. Qin, L. Zheng, Y. Xie, C. Wu, On the framework hydroxyl
633 groups of H-ZSM-5 zeolites, *Journal of Catalysis*. 95 (1985) 609–
634 612. [https://doi.org/10.1016/0021-9517\(85\)90140-X](https://doi.org/10.1016/0021-9517(85)90140-X).
- 635 [30] F. Holzer, U. Roland, F.D. Kopinke, Combination of non-thermal
636 plasma and heterogeneous catalysis for oxidation of volatile
637 organic compounds. Part 1. Accessibility of the intra-particle
638 volume, *Applied Catalysis B: Environmental*. 38 (2002) 163–181.
639 [https://doi.org/10.1016/S0926-3373\(02\)00040-1](https://doi.org/10.1016/S0926-3373(02)00040-1).
- 640 [31] F. Zhang, A.C. Co, L. Olander, E. Wollenberg, F. Tubiello, J.
641 Amouroux, S. Cavadias, A. Doubla, Carbon Dioxide reduction by
642 non-equilibrium electrocatalysis plasma reactor, (n.d.).
643 <https://doi.org/10.1088/1757-899X/19/1/012005>.
- 644 [32] R. V. Siriwardane, M.-S. Shen, E.P. Fisher, J. Losch, Adsorption
645 of CO₂ on Zeolites at Moderate Temperatures, *Energy & Fuels*. 19
646 (2005) 1153–1159. <https://doi.org/10.1021/ef040059h>.
- 647 [33] P.J.E. Harlick, F.H. Tezel, An experimental adsorbent screening
648 study for CO₂ removal from N₂, *Microporous and Mesoporous*
649 *Materials*. 76 (2004) 71–79.
650 <https://doi.org/10.1016/j.micromeso.2004.07.035>.
- 651 [34] X. Fan, S. Kang, J. Li, T. Zhu, Formation of Nitrogen Oxides (N₂O,
652 NO, and NO₂) in Typical Plasma and Plasma-Catalytic Processes
653 for Air Pollution Control, *Water, Air, and Soil Pollution*. 229
654 (2018) 1–12. <https://doi.org/10.1007/s11270-018-4011-y>.
- 655 [35] K. Krawczyk, Conversion of nitrous oxide by positive pulsed
656 corona discharge, *IEEE Transactions on Plasma Science*. 37 (2009)
657 884–889. <https://doi.org/10.1109/TPS.2009.2018261>.
- 658 [36] S. Pekárek, Effect of catalysts on dc corona discharge poisoning,
659 *European Physical Journal D*. 61 (2011) 657–662.
660 <https://doi.org/10.1140/epjd/e2010-10246-4>.
- 661 [37] L.W. Stanek, J.S. Brown, Air Pollution: Sources, Regulation, and
662 Health Effects, Reference Module in Biomedical Sciences. (2019).
663 <https://doi.org/10.1016/B978-0-12-801238-3.11384-4>.
- 664 [38] J. Li, H. Zhang, D. Ying, Y. Wang, T. Sun, J. Jia, In Plasma
665 Catalytic Oxidation of Toluene Using Monolith CuO Foam as a
666 Catalyst in a Wedged High Voltage Electrode Dielectric Barrier
667 Discharge Reactor: Influence of Reaction Parameters and

- 668 Byproduct Control, International Journal of Environmental
669 Research and Public Health. 16 (2019) 711.
670 <https://doi.org/10.3390/ijerph16050711>.
- 671 [39] O. Karatum, M.A. Deshusses, A comparative study of dilute VOCs
672 treatment in a non-thermal plasma reactor, Chemical Engineering
673 Journal. 294 (2016) 308–315.
674 <https://doi.org/10.1016/j.cej.2016.03.002>.
- 675 [40] C. Zhao, H. Deng, Y. Li, Z. Liu, Photodegradation of
676 oxytetracycline in aqueous by 5A and 13X loaded with TiO₂ under
677 UV irradiation, Journal of Hazardous Materials. 176 (2010) 884–
678 892. <https://doi.org/10.1016/j.jhazmat.2009.11.119>.
- 679 [41] M.M.J. Treacy, J.B. Higgins, Collection of simulated XRD powder
680 patterns for zeolites, 2007.
- 681 [42] C. Ramakrishna, B.K. Saini, K. Racharla, S. Gujarathi, C.S.
682 Sridara, A. Gupta, G. Thakkallapalli, P.V.L. Rao, Rapid and
683 complete degradation of sulfur mustard adsorbed on M/zeolite-13X
684 supported (M = 5 wt% Mn, Fe, Co) metal oxide catalysts with
685 ozone, RSC Advances. 6 (2016) 90720–90731.
686 <https://doi.org/10.1039/c6ra17215f>.
- 687 [43] K.M. Valkaj, A. Katović, S. Zrnčević, Catalytic properties of
688 Cu/13X zeolite based catalyst in catalytic wet peroxide oxidation
689 of phenol, Industrial and Engineering Chemistry Research. 50
690 (2011) 4390–4397. <https://doi.org/10.1021/ie102223g>.
- 691 [44] C. Zhou, A. Alshameri, C. Yan, X. Qiu, H. Wang, Y. Ma,
692 Characteristics and evaluation of synthetic 13X zeolite from
693 Yunnan's natural halloysite, Journal of Porous Materials. 20 (2013)
694 587–594. <https://doi.org/10.1007/s10934-012-9631-9>.
- 695 [45] M.A. Hernández, L. Corona, A.I. Gonzalez, F. Rojas, V.H. Lara, F.
696 Silva, Quantitative study of the adsorption of aromatic
697 hydrocarbons (benzene, toluene, and p-xylene) on dealuminated
698 clinoptilolites, Industrial and Engineering Chemistry Research. 44
699 (2005) 2908–2916. <https://doi.org/10.1021/ie049276w>.
- 700 [46] P.S. Esbah Tabaei, R. Ghobeira, P. Cools, F. Rezaei, A. Nikiforov,
701 R. Morent, N. de Geyter, Comparative study between in-plasma
702 and post-plasma chemical processes occurring at the surface of
703 UHMWPE subjected to medium pressure Ar and N₂ plasma
704 activation, Polymer (Guildf). (2020) 122383.
705 <https://doi.org/10.1016/j.polymer.2020.122383>.
- 706 [47] V.H. Ramos-Martinez, E. Ramirez-Vargas, F.J. Medellin-
707 Rodriguez, C.A. Ávila-Orta, C.A. Gallardo-Vega, A.B. Jasso-
708 Salcedo, M.L. Andrade-Guel, Zeolite 13X modification with
709 gamma-aminobutyric acid (GABA), Microporous and Mesoporous
710 Materials. 295 (2020) 109941.
711 <https://doi.org/10.1016/j.micromeso.2019.109941>.
- 712 [48] R. Vinodh, C. Deviprasath, C.V.V. Muralee Gopi, V.G.
713 Raghavendra Kummara, R. Atchudan, T. Ahamad, H.J. Kim, M.
714 Yi, Novel 13X Zeolite/PANI electrocatalyst for hydrogen and
715 oxygen evolution reaction, International Journal of Hydrogen
716 Energy. (2020). <https://doi.org/10.1016/j.ijhydene.2020.07.194>.
- 717 [49] T.L. Barr, The nature of the relative bonding chemistry in zeolites:
718 An XPS study, Zeolites. 10 (1990) 760–765.
719 [https://doi.org/10.1016/0144-2449\(90\)90058-Y](https://doi.org/10.1016/0144-2449(90)90058-Y).
- 720 [50] X. Wang, C.A. Plackowski, A. V. Nguyen, X-ray photoelectron
721 spectroscopic investigation into the surface effects of sulphuric acid

- 722 treated natural zeolite, *Powder Technology*. 295 (2016) 27–34.
723 <https://doi.org/10.1016/j.powtec.2016.03.025>.
- 724 [51] K.A. Cychosz, R. My Guillet-Nicolas, J. Garcí A-Martí Nez, M.
725 Thommes, Recent advances in the textural characterization of
726 hierarchically structured nanoporous materials, *Chem. Soc. Rev.* 46
727 (2017) 389. <https://doi.org/10.1039/c6cs00391e>.
- 728 [52] Z. Wang, L.A. O’Dell, X. Zeng, C. Liu, S. Zhao, W. Zhang, M.
729 Gaborieau, Y. Jiang, J. Huang, Insight into Three-Coordinate
730 Aluminum Species on Ethanol-to-Olefin Conversion over ZSM-5
731 Zeolites, *Angewandte Chemie*. 131 (2019) 18229–18236.
732 <https://doi.org/10.1002/ange.201910987>.
- 733 [53] G. Li, E.A. Pidko, The Nature and Catalytic Function of Cation
734 Sites in Zeolites: a Computational Perspective, *ChemCatChem*. 11
735 (2019) 134–156. <https://doi.org/10.1002/cctc.201801493>.
- 736 [54] L.P. Teh, S. Triwahyono, A.A. Jalil, R.R. Mukti, M.A.A. Aziz, T.
737 Shishido, Mesoporous ZSM5 having both intrinsic acidic and basic
738 sites for cracking and methanation, *Chemical Engineering Journal*.
739 270 (2015) 196–204. <https://doi.org/10.1016/j.cej.2015.01.084>.
- 740 [55] F. Jin, Y. Li, A FTIR and TPD examination of the distributive
741 properties of acid sites on ZSM-5 zeolite with pyridine as a probe
742 molecule, *Catalysis Today*. 145 (2009) 101–107.
743 <https://doi.org/10.1016/j.cattod.2008.06.007>.
- 744 [56] S. Alejandro, H. Valdés, M.H. Manéro, C.A. Zaror, Oxidative
745 regeneration of toluene-saturated natural zeolite by gaseous ozone:
746 The influence of zeolite chemical surface characteristics, *Journal of*
747 *Hazardous Materials*. 274 (2014) 212–220.
748 <https://doi.org/10.1016/j.jhazmat.2014.04.006>.
- 749 [57] S. Schallmoser, T. Ikuno, M.F. Wagenhofer, R. Kolvenbach, G.L.
750 Haller, M. Sanchez-Sanchez, J.A. Lercher, Impact of the local
751 environment of Brønsted acid sites in ZSM-5 on the catalytic
752 activity in n-pentane cracking, *Journal of Catalysis*. 316 (2014) 93–
753 102. <https://doi.org/10.1016/j.jcat.2014.05.004>.
- 754 [58] H. Valdés, V.A. Solar, E.H. Cabrera, A.F. Veloso, C.A. Zaror,
755 Control of released volatile organic compounds from industrial
756 facilities using natural and acid-treated mordenites: The role of
757 acidic surface sites on the adsorption mechanism, *Chemical*
758 *Engineering Journal*. 244 (2014) 117–127.
759 <https://doi.org/10.1016/j.cej.2014.01.044>.
- 760 [59] Z. Ye, S.K.P. Veerapandian, I. Onyshchenko, A. Nikiforov, N. de
761 Geyter, J.-M. Giraudon, J.-F. Lamonier, R. Morent, An in-Depth
762 Investigation of Toluene Decomposition with a Glass Beads-
763 Packed Bed Dielectric Barrier Discharge Reactor, *Industrial and*
764 *Engineering Chemistry Research*. 56 (2017).
765 <https://doi.org/10.1021/acs.iecr.7b00963>.
- 766 [60] T. Yin, X. Meng, L. Jin, C. Yang, N. Liu, L. Shi, Prepared
767 hydrophobic Y zeolite for adsorbing toluene in humid environment,
768 *Microporous and Mesoporous Materials*. 305 (2020) 110327.
769 <https://doi.org/10.1016/j.micromeso.2020.110327>.
- 770